IOP Publishing Journal of Optics
J. Opt. 18 (2016) 065105 (11pp) doi:10.1088/2040-8978/18/6/065105

Reproduction and optical analysis of *Morpho*-inspired polymeric nanostructures

Cary A Tippets[1], Yulan Fu[2], Anne-Martine Jackson[3], Eugenii U Donev[4] and Rene Lopez[2]

[1] Department of Applied Physical Sciences, University of North Carolina at Chapel Hill, NC 27599, USA
[2] Department of Physics and Astronomy, University of North Carolina at Chapel Hill, NC 27599, USA
[3] Department of Chemistry, University of North Carolina at Chapel Hill, NC 27599, USA
[4] Department of Physics and Astronomy, The University of the South, Sewanee, TN 37383, USA

E-mail: rln@physics.unc.edu

Received 6 January 2016, revised 16 March 2016
Accepted for publication 30 March 2016
Published 11 May 2016

Abstract

The brilliant blue coloration of the *Morpho rhetenor* butterfly originates from complex nanostructures found on the surface of its wings. The *Morpho* butterfly exhibits strong short-wavelength reflection and a unique two-lobe optical signature in the incident (θ) and reflected (ϕ) angular space. Here, we report the large-area fabrication of a *Morpho*-like structure and its reproduction in perfluoropolyether. Reflection comparisons of periodic and quasi-random 'polymer butterfly' nanostructures show similar normal-incidence spectra but differ in the angular θ–ϕ dependence. The periodic sample shows strong specular reflection and simple diffraction. However, the quasi-random sample produces a two-lobe angular reflection pattern with minimal specular refection, approximating the real butterfly's optical behavior. Finite-difference time-domain simulations confirm that this pattern results from the quasi-random periodicity and highlights the significance of the inherent randomness in the *Morpho*'s photonic structure.

S Online supplementary data available from stacks.iop.org/JOPT/18/065105/mmedia

Keywords: *Morpho* butterfly, polymer replication, bioinspired photonic crystals, photonic nanostructures, structural color

(Some figures may appear in colour only in the online journal)

Introduction

Many living creatures have biological surfaces that exhibit structural colors [1–4]. Examples of these colors can be found on birds [5], beetles [6] and butterflies [7, 8], and are typically identified by their striking iridescence. Structural color is produced by photonic nanostructures varying in shape and complexity, and many have been morphologically and optically characterized [7]. Some of the most interesting photonic structures in nature are found on the wings of the *Morpho* butterflies. The optical behavior of the *Morpho* butterfly genus has piqued the interest of researchers due to its high intensity, color purity, and unique angular response. In particular, the *M. rhetenor* species is known for its amazing blue color (figures 1(a)–(d)) and has been studied in detail [2, 9–11]. The nanostructures responsible for this brilliant color are quasi-periodic ridges (figure 1(e)) whose cross-sections resemble pine trees made of chitin (figure 1(f)). The 'pine-tree' branches (lamellae) on either side of each tree are vertically offset, thus producing asymmetric structures. Each pine-tree ridge randomly varies in height and lateral spacing from its neighbors. This hierarchical arrangement is often referred to as an 'ultrastructure'. The alternating lamellae-and-air stack of the ultrastructure gives rise to a multilayer interference effect, which regulates the wavelength of reflected light [7, 9, 12–15]. The color purity across a wide range of viewing angles is enabled by the quasi-periodicity of the structures, which causes the light to spread [16]. Diffraction effects are smeared out due to irregularity in the height of the ultrastructures and the asymmetry of each individual tree

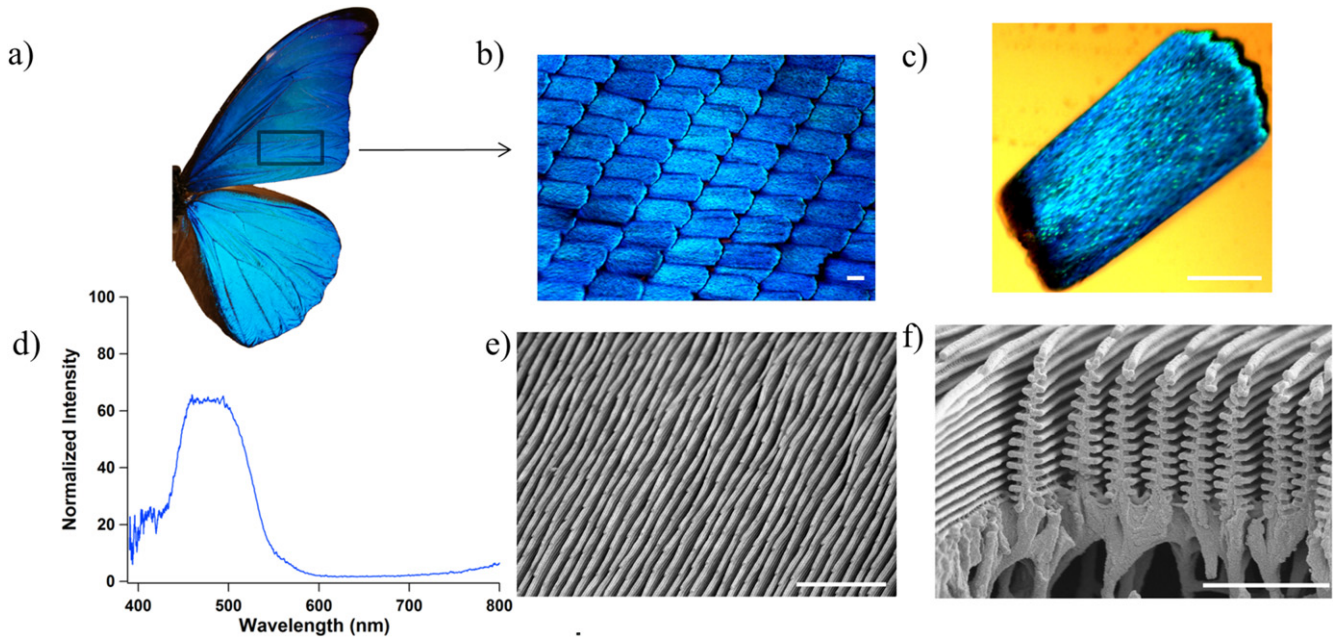

Figure 1. Images of *Morpho rhetenor* butterfly show the various structures found on its wings. (a) Photograph of one half of the butterfly. (b) Optical micrograph of the wing's tilted scales. (c) An individual scale with grating-like structures visible. (d) Reflection spectrum of the *Morpho* wing, with an intensity peak between 460 and 500 nm. (e) Scanning electron micrograph (SEM) of quasi-parallel rows with varying heights and periods. (f) Cross-section of the *Morpho* ultrastructures, showing alternating lamellae. Scale bars: (b), (c) 50 μm, (d) 5 μm, (e) 2 μm.

[12, 17, 18]. The irregularity of the structures thus allows each ridge to contribute separately to the overall optical effect.

Artificial photonic structures inspired by the *Morpho* butterfly could exploit these unique optical properties for a variety of applications [19, 20]. *Morpho*-mimetic and simplified nanostructures have been explored for use as high-sensitivity gas [21–23], chemical [24], and temperature sensors [25, 26]. Further advances may allow for tunable structural color to find application in high precision- and broad-color gamut displays, waveguides, non-duplicable security labels and camouflage technology. In order for these applications to possess similar optical sensitivity, *Morpho*-inspired nanostructures must be true to the *Morpho* butterfly's optical and morphological features. The complex shape of the *Morpho* nanostructure increases the difficulty of fabricating these structures. Alternative approaches to produce structural color include rigid and polymeric multilayers [27, 28] or self-assembled colloidal films [29–31]. While these methods can produce intense diffractive colors with strong angular dependence, non-diffractive colors are only observable near the specular reflection. Angle dependence in the reflection spectra of multilayer stacks and colloidal films has been overcome by applying lessons from the *Morpho* butterfly, utilizing variations in height and periodicity to produce structural randomization [32–34]. However, multilayer stacks fail to reproduce the large specific surface area and angular response of the butterfly, limiting the possible applications, such as sensors that require a large surface area to elicit a wavelength response while interacting with gases or liquids.

Attempting to replicate the exact structure of the butterfly, some researchers have used the butterfly wings as a biological template for direct molding [25, 35–38]. This approach accurately reproduces the exact shape of the ultrastructure and the optical response can be tuned by changing the composition or thickness of a deposited coating on top of the butterfly structures. However, the need for the natural template limits the applicability of any such device. Ultrastructures that exhibit optical effects similar to the butterfly's optical response have been demonstrated by direct ion beam writing [39] and e-beam lithography [12, 23], but these methods are limited in scale and avoid the diffraction effects of periodic structures by studying the optics of a few structures. Siddique *et al* recently demonstrated a photolithography method that allows for large-area fabrication and broad angular response for blue light, but the fabrication method does not allow for the introduction of randomness similar to the butterfly to break the periodicity [40].

Here we present the fabrication of *Morpho*-inspired polymeric nanostructures for broad-angle light distribution. For comparison, we present a detailed analysis of the *M. rhetenor's* angular response over the visible spectrum, showcasing its ability to spread blue light over the entire planar incident and reflection (θ–ϕ, figure 2(a)) angular space and to produce a high-intensity two-lobe θ–ϕ angular signature at its peak reflectance. We show the fabrication and optical characterization of periodic and quasi-periodic ultrastructures made of perfluropolyether (PFPE). The polymer material allows for the introduction of randomness, in order to optically decouple the individual ridges. Periodic and quasi-periodic versions of the artificial butterfly structures differ

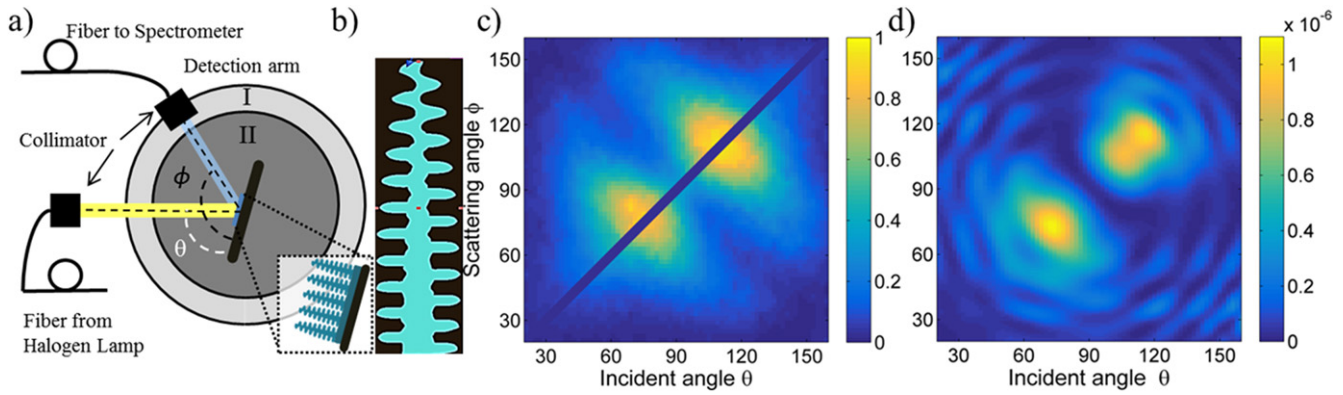

Figure 2. (a) The θ–ϕ experimental setup. For each incident angle (θ, white), a spectrum is taken for a range of reflection angles (ϕ, black) from 10° to 170°; θ and ϕ are measured from the sample's plane. I and II denote rotary stages for detection arm and sample respectively. Inset: nanostructured ridges run perpendicular to the plane of incidence defined by the sample normal and the incident beam. Note: when $\phi = \theta$, no data could be collected due to a limitation in the experimental setup. (b) Simulated *Morpho* 'tree', based on previously reported cross-sectional model [42]. (c) The θ–ϕ sweep at 460 nm of the *M. rhetenor* wing shows regions of strong back-reflection peaking in intensity between 460 and 480 nm. (d) Two-dimensional (2D) FDTD simulations of far-field electric-field intensity scattered at 460 nm from the cross-sectional model of a single *M. rhetenor* ridge, with a similar peak position of the two-lobe optical signature.

substantially in their angular response but have similar normal-reflection spectra, which peak in the region of the real butterfly's color. The strictly periodic samples produce mostly specular reflection with first-order diffraction and minor scattering. Introduction of disorder in the nanostructures produces a wider, two-lobe θ–ϕ angular response. Finite-difference time-domain (FDTD) simulations were used throughout the study to confirm the origin of the optical features observed in the experimental samples.

Experimental section

PFPE synthesis

1 g (1 mmol) PFPE (Solvay Solexis) was dissolved in 50 ml dry methylene chloride. Triethylamine (2 mmol, 0.2 g) was dropwise added to the solution at 0 °C. 2-Isocyanatoethyl methacrylate (2.1 mmol, 0.33 g) (TCI America) was added to the solution and stirred overnight at room temperature. The solution was filtered, and remaining solvent was removed by rotary evaporation. The product was purified by washing with toluene, centrifugation and then drying *in vacuo* at room temperature.180 MPa PFPE was made by mixing 1 k PFPE with 1,1,5,5-tetrahydroperfluoro-1, 5 pentanediol dimethacrylate monomer at a ratio of 1:3. The solution was then mixed with 2% w/v of photointiator 2,2-diethoxyacetophenone.

Fabrication of PFPE structures

The PFPE solution was poured over the Si_3N_4/SiO_2 nanostructured hard master, and degassed in a desiccator for 30 min. The polymer was cross-linked under 365 nm light for 5 min in a nitrogen atmosphere. The cross-linked PFPE and hard master were then placed in 48% HF acid solution for several hours until the hard master was completely destroyed. Periodic-tree samples were kept submerged in water, and then transferred to a water–ethanol solution, gradually increasing the concentration until the sample was submerged in a 100%-ethanol bath. Subsequently, the sample was transferred to a Tousimis Semidri PVT-3 critical point dryer and immersed in liquid CO_2. After supercritical drying, the sample was separated from the remaining Si substrate of the hard master. For the quasi-periodic nanostructures, the sample was immediately removed from the acid solution and cleaned in deionized water. The PFPE replica and Si substrate were separated and the PFPE replica allowed to dry in air.

θ–ϕ measurements

Angular optical measurements were taken for incident and reflected beams both ranging from 10° to 170° with a resolution of 2°. The incident angle was changed by adjusting the sample angle using a rotary stage, while a second rotary stage, rotated 160° about each incident angle, controlled the angle of collection. An unpolarized halogen light source with a 2 mm diameter spot size was used to illuminate the sample and a Princeton Instruments SpectraPro 2300i spectrograph with a Pixis 400 CCD collected the visible spectrum for each angle. Samples were aligned, such that ridges ran vertical to the plane of the sample. The *M. rhetenor* butterfly specimen was ordered from ButterflyUtopia.com.

Normal-incidence reflection measurements

A halogen lamp was used to illuminate the sample surface. Reflection measurements were taken at normal incidence and collected with a 20× objective lens with a 0.4 numerical aperture resulting in a collection cone of 46°. Spectra were normalized using reflected light from an aluminum-coated mirror. Reflected light was analyzed with an Ocean Optics USB4000 spectrometer.

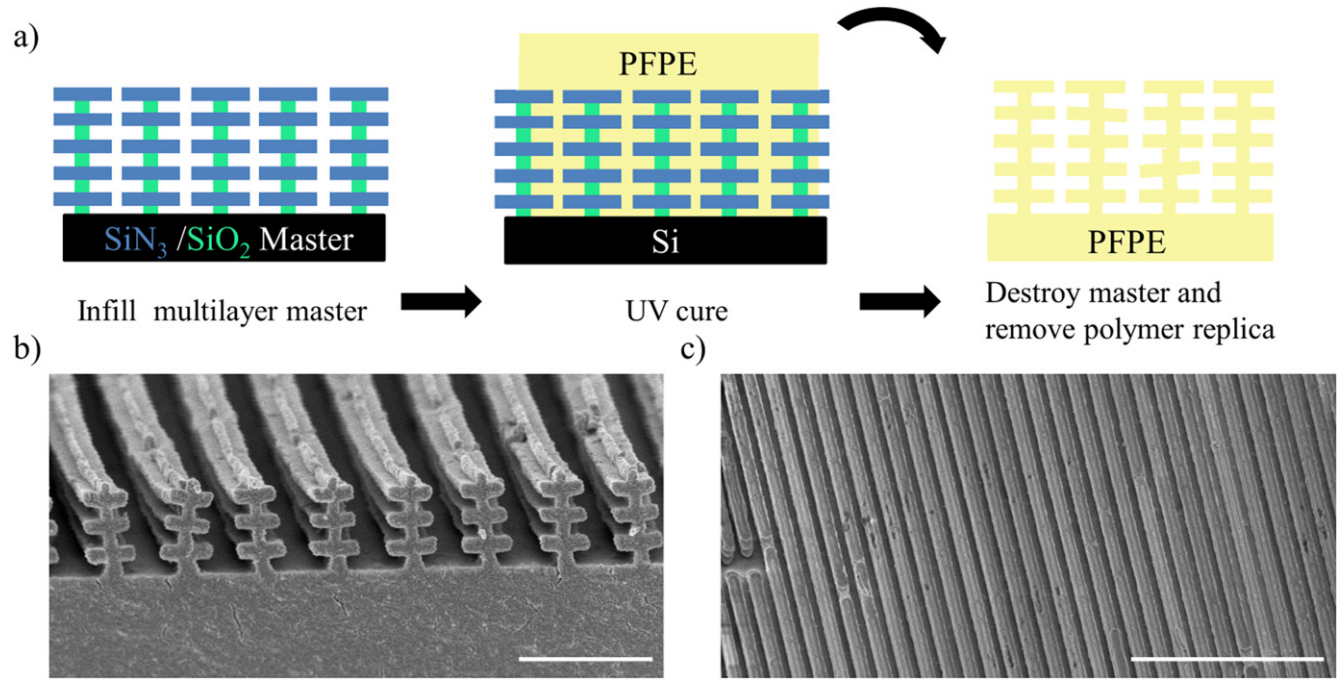

Figure 3. Polymer replica process for *Morpho*-inspired ultrastructures. (a) The SiO_2 and Si_3N_4 master is infilled with PFPE and cross-linked under UV radiation. The master is then etched away in a hydrofluoric acid bath and the resulting PFPE replica is separated from the remaining Si substrate, followed by supercritical drying or air drying. (b) Cross-section of supercritically-dried periodic polymer ultrastructures. (c) Aerial view of the periodic replica ridges. Scale bars: (b) 1 μm and (c) 5 μm.

FDTD simulations

FDTD computer simulations were performed using the commercial software package FDTD Solutions (ver. 8.12.501 by Lumerical Solutions, Inc.) on a single workstation with two octa-core 2.0 GHz processors and 64 GB memory. Each set of 2D simulations consisted of nested sweeps of the illumination parameters: incident angle ($\theta = 20°$–$160°$, $\Delta\theta = 2°$), electric-field polarization (transverse electric and transverse magnetic, TE and TM), and wavelength (one or more values within $\lambda = 400$–520 nm). The largest sets contained close to 1000 individual simulations and ran for about 24 h, including far-field post-processing. The scattering object (s), i.e. one or more *Morpho*-like (figure 2(b)) or *Morpho*-mimetic (figures 4(b) and 8(a), (e), (i)) 'trees' in vacuum (figure 2) or on a substrate of the same refractive index, were placed inside a 2D computational domain ($20 \times 2\ \mu m^2$) surrounded by absorbing boundaries of 80 uniaxial perfectly matched layers (UPML). The refractive index of the *Morpho*-like structure was taken as 1.55 [42]; the (quasi-)periodic structures were assigned a refractive index of 1.30. The domain was meshed globally with a non-uniform conformal mesh, while a smaller rectangular region containing the scatterer(s) was meshed locally at uniform 5 nm increments in both directions. A total-field/scattered-field (TF/SF) source region spanning the inside of the overriding local mesh injected a monochromatic plain wave down from ~50 nm above the scatterer(s). With the incident electromagnetic field removed by the output boundaries of the TF/SF source, only the near-zone fields scattered by the object(s) were collected by a horizontal line monitor placed ~100 nm above the object (s) and cutting across the full domain and side UPML boundaries. The time-dependent near fields collected by the monitor were first Fourier-transformed into frequency space, and then transformed to the far (radiation) zone (here: 1 m away from the origin in the upper hemisphere) at different scattering angles ($\phi = 20°$–$160°$, $\Delta\phi = 1°$). At each wavelength of interest, the squares of the magnitudes of the complex electric far fields for TE and TM incident polarizations were added together, and the resulting far-field 'intensity' ($|\tilde{E}_{far}|^2$) was plotted on a ϕ-versus-θ color-scaled image as a function of scattering and incident angles.

Results and discussion

Morpho rhetenor

The *M. rhetenor*'s ability to spread light cannot be fully appreciated without further exploring the dependence on incident angle and wavelength. θ–ϕ measurements have been shown to present an informative physical description of the angular color response [41]. To explore this relationship, angular measurements were taken from 10° to 170° for both incident and reflected light with an angular resolution of 2°. The incident angle was changed by adjusting the sample angle using a rotary stage, while a second rotary stage controlled the angle of collection, rotating 160° about each incident angle. A schematic of the θ–ϕ measurement setup is presented in figure 2(a).

A double-angle measurement for each wavelength was compiled and shown in video S1 (Supporting Information).

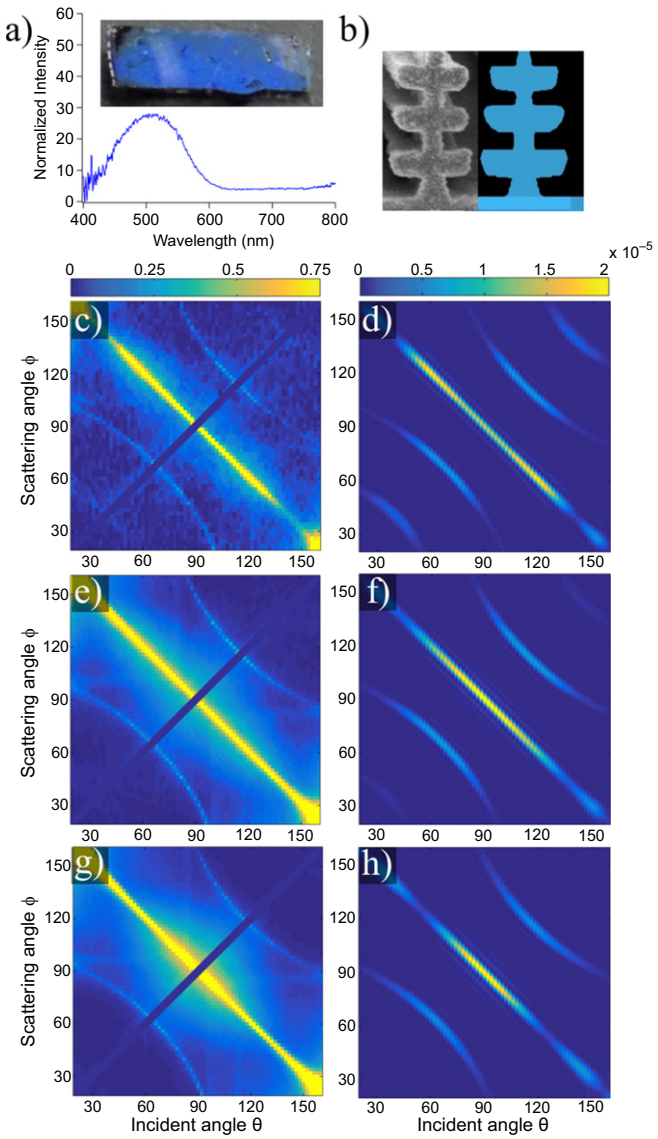

Figure 4. (a) Reflection spectrum of periodic *Morpho*-mimetic periodic polymer nanostructures. Inset: photograph of PFPE replica's specular reflection taken under ambient light. Image dimensions: 25 mm × 10 mm (b) SEM cross-section of a single ultrastructure and the symmetrized version used for FDTD simulations. (c), (e), (g) θ–ϕ measurements of the periodic nanostructures for wavelengths 430, 470 and 520 nm, and (d), (f), (h) corresponding FDTD simulations of nine three-branch nanostructures spaced laterally by 575 nm. Note: when $\phi = \theta$, no data could be collected due to a limitation in the experimental setup.

The video shows that short wavelengths spread over large angles, while the peak-intensity wavelengths concentrate the reflected (scattered) light into the two-lobe feature. Figure 2(b) shows the θ–ϕ angular measurement at 460 nm for the *M. rhetenor*. At short wavelengths (400–430 nm), the light is spread out over a large range of incident and reflected angles. For wavelengths longer than 430 nm, the intensity pattern begins to coalesce within smaller angular ranges and forms the high-intensity two-lobe pattern, as shown previously [42]. The intensity of the patterns peaks between 460 and 500 nm and then begins to dissipate. FDTD simulations (figure 2(c)) of a single *Morpho* ultrastructure qualitatively reproduce this pattern, with angular position and general shape of the central peaks similar to those found experimentally. This somewhat surprising result holds true because the ridges on the butterfly's wing scales exhibit some randomness in their geometry (ridge height, spacing, and 'waviness'; e.g., see figures 1(e) and (f)), which optically decouples each ridge from its neighbors and effectively renders each scale and, in turn, the whole wing into an ensemble of incoherent scatterers. The concentric ring features in the FDTD θ–ϕ pattern are the only difference between the simulation and the real butterfly. Testing variations in the structure (not shown), we noticed that those rings are much more dependent on the ultrastructure's geometrical aspects than are the bright lobes, thus the real butterfly, with its millions of non-identical ridges, must average out the rings effectively. Overall, the simulation indicates that each ultrastructure row on the scales of the butterfly contributes incoherently to the optical signature without undergoing significant interference with neighboring ultrastructures [43]. This θ–ϕ pattern illustrates the challenge of artificial reproduction of the *Morpho* color characteristics, highlighting the need for decoupling the ultrastructures while simultaneously maintaining parallel nanofabrication.

Periodic nanostructures

Polymer nanostructures were fabricated using a silicon master as a sacrificial mold, consisting of a silicon nitride and silicon oxide multilayer thin-film stack on a silicon substrate, as illustrated in figure 3(a). Fabrication of the hard master has been reported previously [44]. Besides optimizing the master to reflect in the visible part of the spectrum and to increase the intensity of the reflected light, by increasing the lamellae length, decreasing the size of the ultrastructure base and decreasing the periodicity, we also intended to transfer the photonic structure to a single transparent polymer material with varying replication fidelity in order to investigate the effect of imperfect ridge to ridge periodicity. The silicon master fabrication process was designed to produce 1 in^2 samples. Perfluoropolyether (PFPE) was chosen to replicate the butterfly ultrastructures due to its optical transparency, refractive index ($n = 1.3$) and high acid resistance. The visible spectrum transparency removes material contributions (i.e., absorption) to the optical signature not resulting from the photonic structures. Previous polymer replication resulted in lamellae and base size that limited the optical intensity [44]. Commercially available PFPE was methacraylate-functionalized and blended with a fluorinated monomer in order to increase its Young's modulus. The PFPE solution was poured over the Si_3N_4/SiO_2 hard master and degassed. The polymer was then cross-linked under 365 nm light for 5 min in a nitrogen atmosphere. Cross-linked PFPE and hard master were then placed in 48% hydrofluoric acid (HF) for several hours until the hard master was completely dissolved and separated from the Si substrate. In order to obtain completely periodic nanostructures, the samples were kept submerged in water and gradually transferred to 100% ethanol to dehydrate

the sample. Subsequently, the sample was transferred to a supercritical dryer and submerged in liquid CO_2.

Figures 3(b) and (c) show the resultant nanostructures after supercritical drying. These vertical nanostructures reflect blue-green light that peaks at ~510 nm for normal incidence (figure 4(a)). Reflection measurements were taken at normal incidence and collected with a 20× microscope objective with a full angular collection of 46°. Visual inspection of the sample shows the blue and green colors arise mostly from angles close to the specular reflection (figure 4(a) inset). θ–ϕ angular measurements (figures 4(c), (e) and (g)) show very strong specular reflection (diagonal form top left to bottom right), but also significant diffraction consistent with the sample periodicity, resulting in well-defined arcs in the lower-left and upper-right regions of the θ–ϕ plane. The θ–ϕ angular measurements reveal three main reflection signatures dependent on wavelength. For short wavelengths (400–440 nm), two high-intensity narrow spots appear along the specular reflection line (figure 4(c)). For longer wavelengths, the spots expand toward the sample's normal until they merge (figure 4(e)). The light intensity then further concentrates around the sample's normal (figure 4(g)). This angular response is reproduced fairly well by the 2D FDTD simulations using a finitely periodic array of nine identical ultrastructures based on a SEM cross-section image of the sample (figure 4(b)). Figures 4(d), (f) and (h) show the FDTD simulations at different wavelengths illustrating the three observed regimes. The origin of this angular dependence can be explained by realizing that, in the specular reflection region, the dominant contribution is the multilayer nature of the ultrastructures, which, given their dimensions, will have an enhanced reflection for longer wavelengths at normal incidence and will require incident angles farther from the normal for shorter wavelengths [42]. Consistent with the measurement, the FDTD simulation shows the diffraction arcs are weaker in intensity compared to the specular intensity and their position in the θ–ϕ plane is equally well predicted. While these vertical trees are a simplified model of the butterfly, they successfully reproduce its color. However, due to their strict periodicity, they do not closely reproduce the angular optical response of the natural butterfly. In order to approach it, the strict periodicity needs to be broken.

Quasi-periodic nanostructures

Randomness and asymmetry in the *Morpho* butterfly ultrastructure have been shown to be important for its angular optical signature [16, 45]. By altering the periodicity of the nanostructures, the specularly reflected and diffracted light can be scattered instead. Quasi-periodic nanostructures were fabricated in a similar fashion as the periodic trees described above. However, on removal from the acid solution, the PFPE replica was separated from the remaining silicon substrate and air dried, rather than super critically dried. Figures 5(a)–(c) show representative SEM images of the *Morpho*-mimetic structures. Aerial SEM images of the sample (figures 5(b) and (c)), taken at a 45° tilt, show that the polymer ultrastructures have randomly leaned onto each other, forming a quasi-periodic pattern. Structure randomization occurred due to capillary forces during the air-drying process. The cross-section (figure 5(a)) shows the tapered tree-like structures consisting of five lamella of PFPE forming multilayer stacks with the surrounding air. While this quasi-randomness differs from that seen on the *M. rhetenor*, which is truly uncorrelated, the quasi-randomness produced by capillary forces affects both the height and period of each ultrastructure, which have been shown to be important for producing *Morpho*-mimetic optical response [43, 46, 47]. Visually, the randomized geometry of this sample resulted in a very weak specular reflection but enhanced blue-green color for angles off the mirror observation line (i.e., diagonal from top left to bottom right).

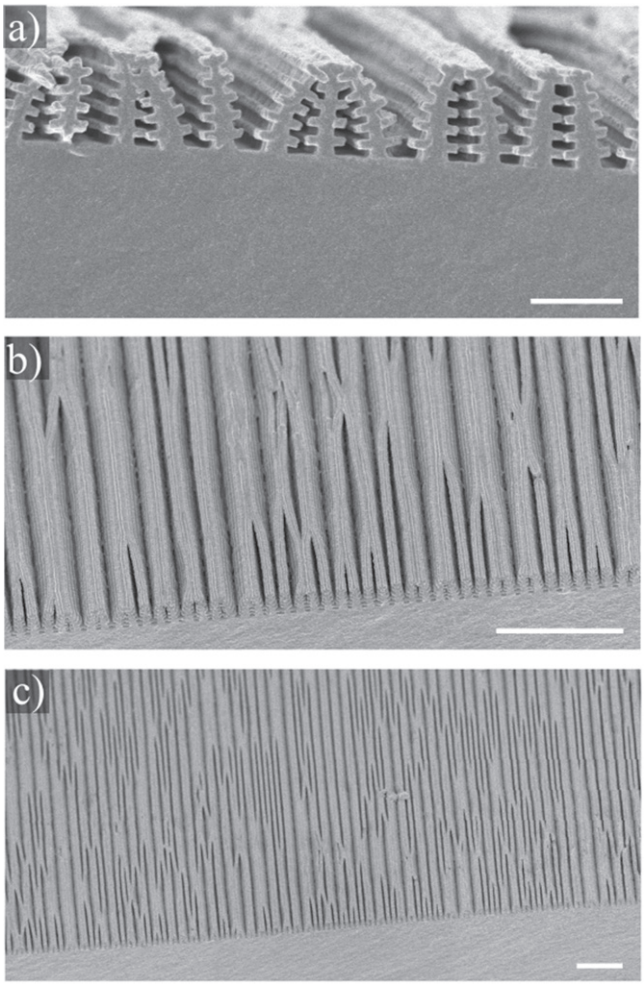

Figure 5. (a) SEM cross-section of the polymeric ultrastructures, with ridges of ultrastructures leaning onto each other after air drying, mainly forming groupings of two and three trees. (b), (c) Aerial SEM images of the replica ridges taken at a 45° tilt for two different magnifications. Ridges bend and stick to each other, introducing randomness to the overall periodicity of the sample. Scale bars: (a) 1 μm; (b), (c) 5 μm.

Figure 6(a) shows the normal-incidence reflection spectrum of the quasi-periodic PFPE structures, with the reflected intensity peaking around 550 nm; a digital photograph of the sample's surface is shown in figure 6(d). The visual differences between the photographs of the quasi-periodic and

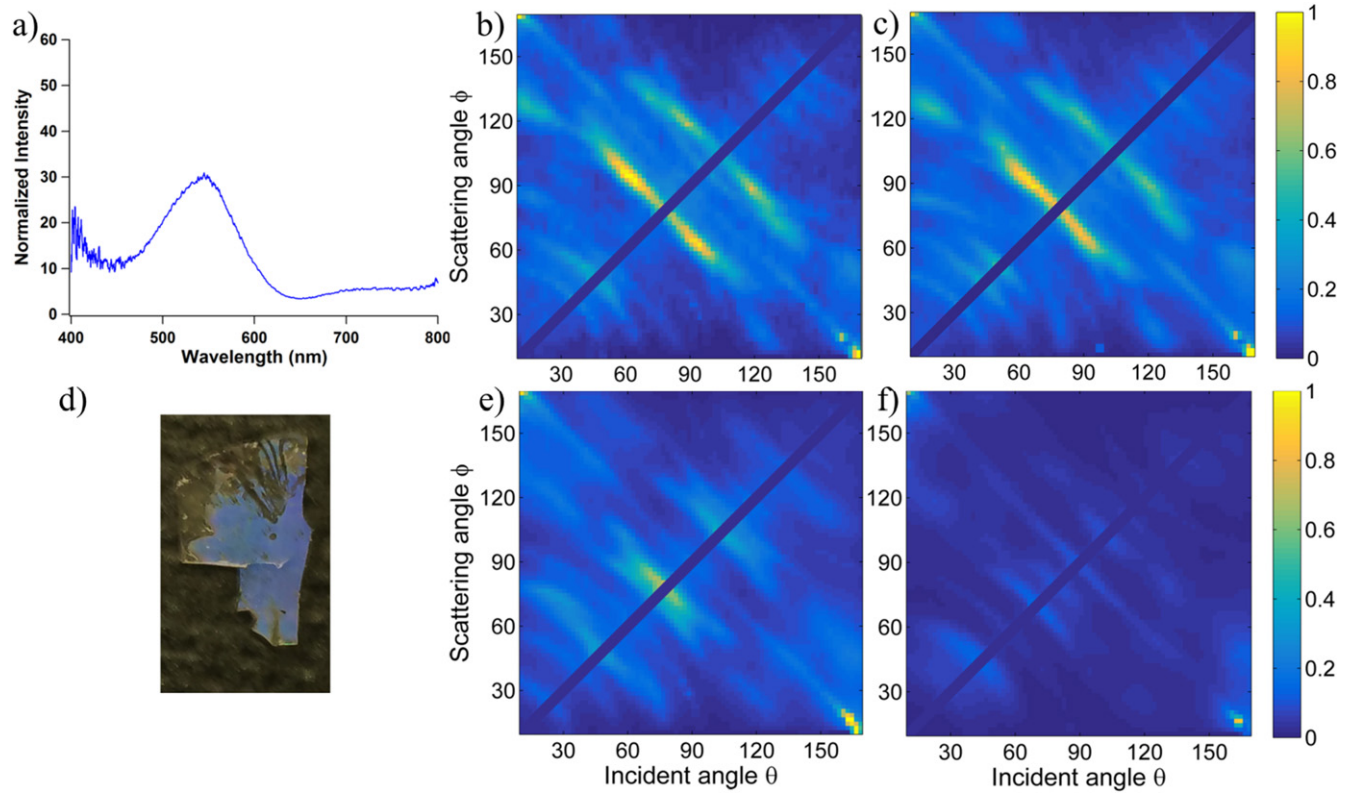

Figure 6. (a) Reflection spectrum of the quasi-periodic PFPE sample. θ–ϕ data for the 'artificial butterfly' sample, taken at various wavelengths. The unique angular response of the quasi-periodic sample is shown for wavelengths (b) 460 nm and (c) 480 nm. (d) A photograph of a quasi-periodic sample, taken under ambient light at $\phi = 90°$, demonstrating the color seen within the two-lobe angular region. Image dimensions: 8 mm $\times$ 13 mm. Beyond 480 nm, the pattern begins to dissipate but first concentrates about 15° away from normal incidence as seen for (e) 520 nm. The pattern intensity decreases until only diffraction lines are visible at (f) 600 nm. Note: when $\phi = \theta$, no data could be collected due to a limitation in the experimental setup.

periodic samples can be attributed to different (i) orientations of the illumination source and camera, (ii) degrees of disorder along the ridges, as many of the quasi-periodic ridges join and split at multiple locations (see figures 5(b) and (c)), and (iii) profiles of the normal-incidence reflection spectra (figure 4(a) versus figure 6(a)). Firstly, the periodic sample was photographed under specular reflection from a fluorescent light incident near 45° (figure 4(a), inset), since its highest reflected intensity lies along the mirror line (see figures 4(c), (e) and (g)), whereas the quasi-periodic sample was photographed directly from above (figure 6(d)), in a dark-field configuration with respect to the fluorescent illumination, in order to collect reflected light away from the low-intensity mirror line (see figures 6(b), (c) and (e)). Secondly, the quasi-periodic sample scatters light out of the plane of incidence due to seemingly random deviations from parallelism along the ridges, which necessarily reduces the brightness of the light reflected into the numerical aperture of the camera lens and renders the sample a duller blue than its periodic counterpart, whose regularity channels most of the reflected light into the zeroth and first diffraction orders. Thirdly, the blue colors of the quasi-periodic and periodic samples are not spectrally identical, as evidenced by the different peak wavelengths of the reflection spectra (~510 nm in figure 4(a) versus ~540 nm in figure 6(a)) and distributions of spectral weight (e.g., compare the 400–500 nm region of each spectrum). In comparison with the natural *Morpho* butterfly, the quasi-periodic sample reflects a paler blue because it lacks the depth (fewer 'branches' per tree: 10 versus 22), the areal density (wider gaps between branches on neighboring trees reduce the reflected intensity), the optical contrast (lower refractive index: $n_{\mathrm{PFPE}} \approx 1.3$ versus $n_{\mathrm{chitin}} \approx 1.55$), and the absorbing layer underneath the ridges, which helps the butterfly purify the blue color by preventing the complementary colors from being reflected from the underlying surface. Clearly, emulating the vivid 'metallic' blue of the brightest *Morpho* species (e.g., *M. rhetenor*) with a patternable polymer remains a challenge, but we believe that our quasi-periodic structures represent a significant step forward.

The angular distribution of the randomized PFPE ultrastructures was measured using the θ–ϕ setup described above. Figures 6(b), (c), (e) and (f) show θ–ϕ measurements at wavelengths of 460 nm, 480 nm, 520 nm and 600 nm, respectively. For the shorter wavelengths, the reflected signal is dominated by high-intensity regions 'sandwiching' the mirror line. The features appear two-lobed and do not match the curving and location of the typical diffraction arcs expected for the nominal period (see figure 4 for the strictly periodic case). At longer wavelengths, the pattern coalesces

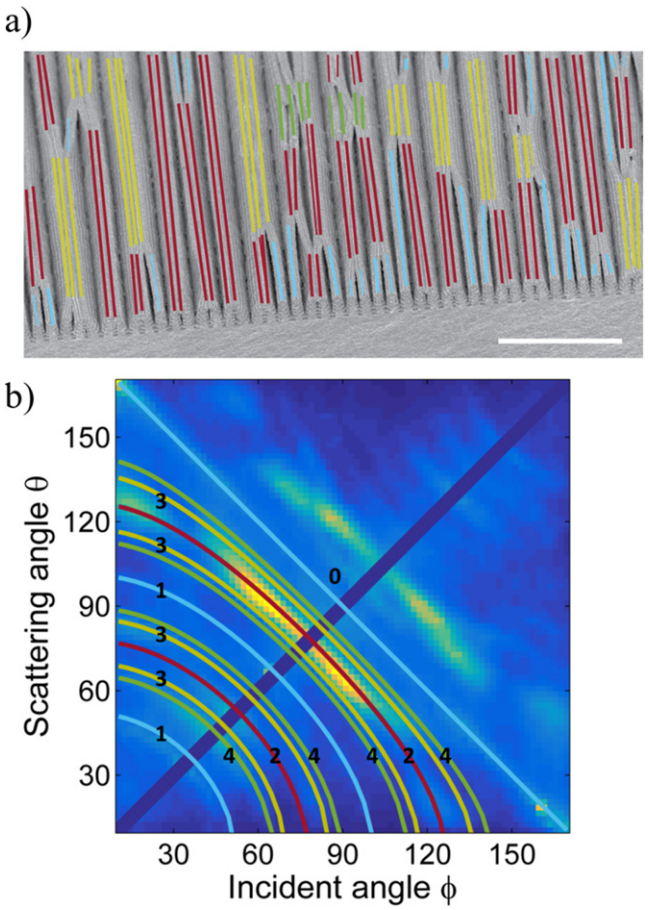

Figure 7. (a) SEM of quasi-periodic surface with lines marking where various combinations contribute. Groupings of two ridges (red) appear to be the most common, with groupings of one (blue), three (yellow) and four (green) ridges also visible. This results in periods of 2, 3 and 4 times the nominal period of 575 nm throughout the sample's surface. (b) θ–ϕ map at 460 nm overlaid with calculated diffraction curves of the 1st, 2nd, 3rd and 4th order of the various periods found on the sample's surface: as-fabricated period (blue, 1), double period (red, 2) triple period (yellow, 3) and quadruple period (green, 4). The high-intensity lobes align predominantly with the double and triple periods. Scale bar: 5 μm.

by first concentrating around $\pm 15^{\circ}$ away from normal incidence before mostly dissipating.

Origin of the optical signature

Further analysis reveals that the optical signature is a product of the quasi-random periodicity formed when the ultrastructures collapse together during air drying. Figure 7(a) highlights the various groupings seen on the surface of the quasi-periodic samples. Nanostructures randomly switch leaning direction against their neighbors and form groups of two, three or four rows. To determine the dominant quasi-periodic structure, diffraction curves (1st, 2nd, 3rd and 4th order) were calculated for grating periodicities of 1, 2, 3 and 4 times the nominal fabrication period (575 nm). These curves are overlaid on the reflection data for a wavelength of 460 nm in figure 7(b). The double-period first-order diffraction arc aligns well with the angular pattern but the arcs from other grating orders seem close enough to possibly contribute, in particular because the overall lobe feature clearly curves the opposite way with respect to the simple diffraction arc. While the angular pattern appears to be a result of quasi-periodicity, it is important to note that the unique angular pattern peaks in intensity around 480 nm, after which the intensity continually dissipates. So, while faint and broad diffraction arcs are visible, the quasi-random structures disrupt the short-range order, such that only blue-green light is reflected. FDTD simulations of the two dominant periods, i.e. two and three rows stuck together, were performed based on SEM cross-sections of the quasi-periodic sample.

In the simulations, the outlines of the trees were made symmetric, as shown in figures 8(a), (e) and (i). Rows of nine, five, and five structures were used, respectively, for single (figure 8(a)), double (figure 8(e)), and triple (figure 8(i)) tree groupings. Convergence tests showed that as few as three units of single, double, or triple ridges already yielded all the features, albeit broader, seen in the corresponding angle-dependent intensity maps in figure 8. Increasing the number of trees sharpened the mirror lines and diffraction arcs, but it did not qualitatively change the angular distributions of the scattered light. Thus, relatively small numbers of simulated scatterers sufficed for the purpose of figure 8, namely to demonstrate that diffraction gratings composed of single as well as pairs and triplets of ridges all contribute to the measured scattering distributions (see, figures 6(b), (c), (e) and (f)), and yet the latter cannot be fully accounted for without including disorder in the long dimension of the ridges (e.g., see figure 7(a)), which would require computationally prohibitive 3D FDTD simulations. The resultant θ–ϕ maps for wavelengths of 460, 480, and 520 nm are shown in the remainder of figure 8. One immediate observation is that contributions from the single period, which shows strong zero-order (i.e., specular reflection) and first-order diffraction, seem to be completely absent in the experimental measurements. The double- and triple-tree simulations show a weaker zero-order reflection, also not seen experimentally. Being two-dimensional, the simulations essentially treat each ridge as infinitely long and the spacing between neighboring ridges as invariant along the suppressed dimension (along the ridge axis). On the other hand, the quasi-periodic sample exhibits marked disorder along the ridges, many of which join and split at multiple locations (e.g., see figure 7(a)). This behavior cannot be captured by the 2D simulations, whereas running the same number ($\sim 10^3$) of 3D FDTD simulations would require either vast computational resources or an unreasonably long time. The 3D ridge disorder leads to diffuse scattering out of the plane of incidence, thus significantly reducing the intensity of the specular reflection measured in the plane. In contrast, the simulated 2D trees scatter light only within the plane of incidence, which is why simulations (figures 4(d), (f) and (h)) and measurements (figures 4(c), (e) and (g)) show very good agreement for the periodic sample (figure 3(b)), whose ridges run parallel and orderly along the third dimension. Furthermore, disorder in the quasi-periodic sample likely creates regions where opposing tree branches

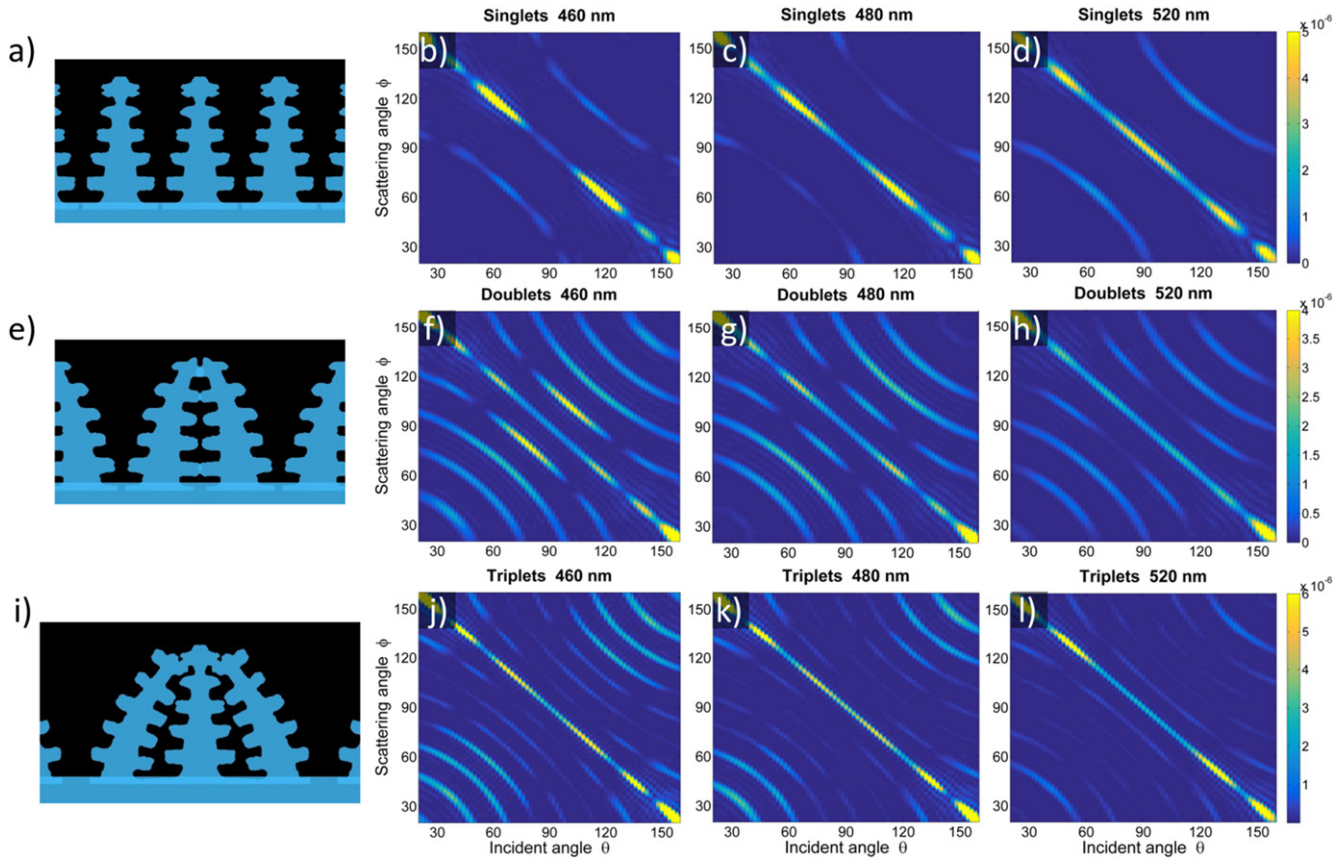

Figure 8. FDTD simulations of nine (singlets) or five (doublets and triplets) symmetric units of representative structure groupings found on the quasi-periodic sample. Schematics of the simulated trees are shown for single trees (a), double trees (e) and triple trees (i). Doublets and triplets were based on SEM cross-sections but symmetrized to simplify the model. θ–ϕ scattered intensity data were simulated and compiled for wavelengths of 460, 480, and 520 nm for each ultrastructure configuration: singlets (b)–(d), doublets (f)–(h), and triplets (j)–(l). A combination of the doublet and triplet simulation (with the exclusion of the nominal period diffraction and specular reflection, not seen experimentally) would explain the unique θ–ϕ two-lobe signature observed for the quasi-periodic sample.

on neighboring ridges are staggered vertically, that is, a branch faces an air gap and vice versa—one of the photonic engineering tricks *Morpho* butterflies employ to extinguish specular reflections [16].

In contrast to the single period, the simulations of the double-tree structure predict high-intensity lobes somewhat reminiscent of the angular distribution of the experimental measurements, as already suggested by the calculated location of the diffraction arc (figure 7(b)). The FDTD simulations show that the arcs are of high intensity near their centers and lose intensity at longer wavelengths, whereas the experimental measurements depict elongated lobes that are more intense toward each end rather than in the middle. The simulations of the triple-tree groupings seem to correspond to the location of some of the weaker diffractive features observed in the experiment, but the intensity difference indicates that the periodic order is fragmented, yet not completely destroyed. Therefore, no grouping alone explains the experimental observations, but combinations of double- and triple-tree structures—varying locally across the sample in their precise *three-dimensional* geometry—are most likely responsible for the signature inward-curving lobes (figures 6(b), (c) and 7(b)) in the experimental optical response of the quasi-periodic 'polymer butterfly'.

Conclusion

The *M. rhetenor* butterfly's structural color was angularly characterized over the visible wavelength range to establish its spectral and angular response characteristics. The butterfly exhibited a unique two-lobe pattern in the θ–ϕ angular space. Nanostructures on the surface of the butterfly's wing are the origin of its optical properties; in particular, the inherent randomness in the photonic structures produces the unique angular signature.

Periodic and quasi-periodic *Morpho*-mimetic nanostructures were produced using microfabrication and soft-polymer replication techniques. These samples were physically and optically characterized in order to explore the relationship between the angular optical signature and randomization in the nanostructures. Both the periodic and quasi-periodic samples exhibited similar normal-incidence reflection spectra but differed dramatically in their angular optical responses. Periodic samples were shown to have angular

dependence dominated by high-intensity specular and diffraction lines, while the quasi-periodic sample produced a two-lobe angular reflection pattern with minimal specular reflection. The measured angular signature of the reflected light of the quasi-periodic ridge ultrastructures followed closely the calculated diffraction lines for the double and triple periodic groupings found on the sample's surface. FDTD simulations offered further evidence that this response results from the quasi-random periodicity of the fabricated nanostructures. This result shows the importance of randomization in the *Morpho* butterfly ultrastructures for producing its unique angular response, especially the randomization in the period of ultrastructure ridges. Furthermore, the introduction of relatively minor randomization in the polymer samples produced a reflection distribution with a similar two-lobe reflection to that of the *M. rhetenor*, highlighting the sensitivity of the angular response to the underlying order of the surface structures. Deliberate introduction of strongly randomized features would allow for more precise control of the angular response.

Acknowledgments

This material is based upon work funded by the National Science Foundation under award number DMR-1243590. The authors thank the Chapel Hill Analytical and Nanofabrication facilities (CHANL) for providing expertise and access to fabrication and analytical equipment. E U Donev gratefully acknowledges start-up funding from the University of the South and computational resources provided by the University's Library and Information Technology Services (LITS).

References

[1] McPhedran R C and Parker A R 2015 Biomimetics: lessons on optics from nature's school *Phys. Today* **68** 32–7
[2] Vukusic P and Sambles J R 2003 Photonic structures in biology *Nature* **424** 852–5
[3] Vigneron J P and Simonis P 2012 Natural photonic crystals *Physica* B **407** 4032–6
[4] Parker A R 2000 515 Million years of structural colour *J. Opt. A*: *Pure Appl. Opt.* **2** R15–28
[5] Stavenga D G, Leertouwer H L, Marshall N J and Osorio D 2011 Dramatic colour changes in a bird of paradise caused by uniquely structured breast feather barbules *Proc. Biol. Sci.* **278** 2098–104
[6] Simonis P and Vigneron J P 2011 Structural color produced by a three-dimensional photonic polycrystal in the scales of a longhorn beetle: pseudomyagrus waterhousei (Coleoptera: Cerambicidae) *Phys. Rev.* E **83** 011908
[7] Kinoshita S and Yoshioka S 2005 Structural colors in nature: the role of regularity and irregularity in the structure *ChemPhysChem* **6** 1442–59
[8] Ghiradella H 1991 Light and color on the wing: structural colors in butterflies and moths *Appl. Opt.* **30** 3492–500
[9] Zhu D, Kinoshita S, Cai D and Cole J 2009 Investigation of structural colors in Morpho butterflies using the nonstandard-finite-difference time-domain method: effects of alternately stacked shelves and ridge density *Phys. Rev.* E **80** 051924
[10] Yoshioka S and Kinoshita S 2004 Wavelength-selective and anisotropic light-diffusing scale on the wing of the Morpho butterfly *Proc. Biol. Sci.* **271** 581–7
[11] Lee R T and Smith G S 2009 Detailed electromagnetic simulation for the structural color of butterfly wings *Appl. Opt.* **48** 4177–90
[12] Siddique R H, Diewald S, Leuthold J and Hölscher H 2013 Theoretical and experimental analysis of the structural pattern responsible for the iridescence of Morpho butterflies *Opt. Express* **21** 14351–61
[13] Steindorfer M A, Schmidt V, Belegratis M, Stadlober B and Krenn J R 2012 Detailed simulation of structural color generation inspired by the Morpho butterfly *Opt. Express* **20** 21485–94
[14] Smith G S 2009 Structural color of Morpho butterflies *Am. J. Phys.* **77** 1010
[15] Banerjee S, Cole J B and Yatagai T 2007 Colour characterization of a Morpho butterfly wing-scale using a high accuracy nonstandard finite-difference time-domain method *Micron* **38** 97–103
[16] Kinoshita S, Yoshioka S and Miyazaki J 2008 Physics of structural colors *Rep. Prog. Phys.* **71** 076401
[17] Kinoshita S, Yoshioka S and Kawagoe K 2002 Mechanisms of structural colour in the Morpho butterfly: cooperation of regularity and irregularity in an iridescent scale *Proc. Biol. Sci.* **269** 1417–21
[18] Johansen V E 2014 Optical role of randomness for structured surfaces *Appl. Opt.* **53** 2405–15
[19] Kumar R, Smith S, Mcneilan J, Keeton M, Sanders J, Talamo A, Bowman C and Xie Y Butterfly wing-inspired nanotechnology *The Nanobiotechnology Handbook* ed Y Xie (Boca Taon: CRC Press) pp 203–22
[20] Zhang W, Gu J, Liu Q, Su H, Fan T and Zhang D 2014 Butterfly effects: novel functional materials inspired from the wings scales *Phys. Chem. Chem. Phys.* **16** 19767–80
[21] Wang F, Meng Z, Xue F, Xue M, Lu W, Chen W, Wang Q and Wang Y 2014 Responsive photonic crystal for the sensing of environmental pollutants *Trends Environ. Anal. Chem.* **3-4** 1–6
[22] Han Z, Niu S, Yang M, Mu Z, Li B, Zhang J, Ye J and Ren L 2010 Unparalleled sensitivity of photonic structures in butterfly wings *RSC Adv.* **4** 45214–9
[23] Potyrailo R A *et al* 2015 Towards outperforming conventional sensor arrays with fabricated individual photonic vapour sensors inspired by Morpho butterflies *Nat. Commun.* **6** 7959
[24] Yang X, Peng Z, Zuo H, Shi T and Liao G 2011 Using hierarchy architecture of Morpho butterfly scales for chemical sensing: experiment and modeling *Sensors Actuators* A **167** 367–73
[25] Lu T, Zhu S, Ma J, Lin J, Wang W, Pan H, Tian F, Zhang W and Zhang D 2015 Bioinspired thermoresponsive photonic polymers with hierarchical structures and their unique properties *Macromol. Rapid Commun.* **36** 1722–8
[26] Pris A D, Utturkar Y, Surman C, Morris W G, Vert A, Zalyubovskiy S, Deng T, Ghiradella H T and Potyrailo R A 2012 Towards high-speed imaging of infrared photons with bio-inspired nanoarchitectures *Nat. Photon.* **6** 195–200
[27] Sveinbjörnsson B R, Weitekamp R A, Miyake G M, Xia Y, Atwater H A and Grubbs R H 2012 Rapid self-assembly of brush block copolymers to photonic crystals *Proc. Natl Acad. Sci. USA* **109** 14332–6
[28] Miyake G M, Weitekamp R A, Piunova V A and Grubbs R H 2012 Synthesis of isocyanate-based brush block copolymers and their rapid self-assembly to infrared-reflecting photonic crystals *J. Am. Chem. Soc.* **134** 14249–54

[29] Fudouzi H and Sawada T 2006 Photonic rubber sheets with tunable color by elastic deformation *Langmuir* **22** 1365–8
[30] Ito T, Katsura C, Sugimoto H, Nakanishi E and Inomata K 2013 Strain-responsive structural colored elastomers by fixing colloidal crystal assembly *Langmuir* **29** 13951–7
[31] Kim S-H, Lee S Y, Yang S-M and Yi G-R 2011 Self-assembled colloidal structures for photonics *NPG Asia Mater.* **3** 25–33
[32] Saito A, Miyamura Y, Ishikawa Y, Murase J, Akai-Kasaya M and Kuwahara Y 2009 Reproduction, mass-production and control of the Morpho-butterfly's blue *Adv. Fabr. Technol. Micro/Nano Opt. Photonics II* **7205** 720506–9
[33] Song B, Eom S C and Shin J H 2014 Disorder and broad-angle iridescence from Morpho-inspired structures *Opt. Express* **22** 19386–400
[34] Zhang Y, Dong B, Chen A, Liu X, Shi L and Zi J 2015 Using cuttlefish ink as an additive to produce non-iridescent structural colors of high color visibility *Adv. Mater.* **27** 4719–24
[35] Huang J, Wang X and Wang Z L 2006 Controlled replication of butterfly wings for achieving tunable photonic properties *Nano Lett.* **6** 2325–31
[36] Kang S-H, Tai T-Y and Fang T-H 2010 Replication of butterfly wing microstructures using molding lithography *Curr. Appl. Phys.* **10** 625–30
[37] Knez M, Nielsch K and Niinistö L 2007 Synthesis and surface engineering of complex nanostructures by atomic layer deposition *Adv. Mater.* **19** 3425–38
[38] Liu F, Liu Y, Huang L, Hu X, Dong B, Shi W, Xie Y and Ye X 2011 Replication of homologous optical and hydrophobic features by templating wings of butterflies Morpho menelaus *Opt. Commun.* **284** 2376–81
[39] Watanabe K, Hoshino T, Kanda K, Haruyama Y, Kaito T and Matsui S 2005 Optical measurement and fabrication from a Morpho-butterfly-scale quasistructure by focused ion beam chemical vapor deposition *J. Vac. Sci. Technol.* B **23** 570
[40] Siddique R H, Faisal A, Hünig R, Bartels C, Wacker I, Lemmer U and Hölscher H 2014 Utilizing laser interference lithography to fabricate hierarchical optical active nanostructures inspired by the blue Morpho butterfly *Proc. SPIE* **9187** 91870E
[41] Kambe M, Zhu D and Kinoshita S 2011 Origin of retroreflection from a wing of the morpho butterfly *J. Phys. Soc. Japan* **80** 1–10
[42] Okada N, Zhu D, Cai D, Cole J B, Kambe M and Kinoshita S 2012 Rendering Morpho butterflies based on high accuracy nano-optical simulation *J. Opt.* **42** 25–36
[43] Saito A, Yonezawa M, Murase J, Juodkazis S, Mizeikis V, Akai-Kasaya M and Kuwahara Y 2011 Numerical analysis on the optical role of nano-randomness on the Morpho butterfly's scale *J. Nanosci. Nanotechnol.* **11** 2785–92
[44] Aryal M, Ko D-H, Tumbleston J R, Gadisa A, Samulski E T and Lopez R 2012 Large area nanofabrication of butterfly wing's three dimensional ultrastructures *J. Vac. Sci. Technol.* B **30** 061802
[45] Chung K *et al* 2012 Flexible, angle-independent, structural color reflectors inspired by morpho butterfly wings *Adv. Mater.* **24** 2375–9
[46] Saito A, Ishikawa Y, Miyamura Y, Akai-Kasaya M and Kuwahara Y 2007 Optimization of reproduced morpho-blue coloration *SPIE Proc.* **6767** 676706
[47] Boulenguez J, Berthier S and Leroy F 2012 Multiple scaled disorder in the photonic structure of Morpho rhetenor butterfly *Appl. Phys.* A **106** 1005–11